

Fabrication, characterisation and analytical modelling of gradient auxetic closed cell foams

DUNCAN, Olly <<http://orcid.org/0000-0001-9503-1464>>, ALDERSON, Andrew <<http://orcid.org/0000-0002-6281-2624>> and ALLEN, Tom <<http://orcid.org/0000-0003-4910-9149>>

Available from Sheffield Hallam University Research Archive (SHURA) at:

<https://shura.shu.ac.uk/28069/>

This document is the Accepted Version [AM]

Citation:

DUNCAN, Olly, ALDERSON, Andrew and ALLEN, Tom (2021). Fabrication, characterisation and analytical modelling of gradient auxetic closed cell foams. *Smart Materials and Structures*. [Article]

Copyright and re-use policy

See <http://shura.shu.ac.uk/information.html>

ACCEPTED MANUSCRIPT

Fabrication, characterisation and analytical modelling of gradient auxetic closed cell foams

To cite this article before publication: Olly Duncan *et al* 2021 *Smart Mater. Struct.* in press <https://doi.org/10.1088/1361-665X/abdc06>

Manuscript version: Accepted Manuscript

Accepted Manuscript is “the version of the article accepted for publication including all changes made as a result of the peer review process, and which may also include the addition to the article by IOP Publishing of a header, an article ID, a cover sheet and/or an ‘Accepted Manuscript’ watermark, but excluding any other editing, typesetting or other changes made by IOP Publishing and/or its licensors”

This Accepted Manuscript is © 2020 IOP Publishing Ltd.

During the embargo period (the 12 month period from the publication of the Version of Record of this article), the Accepted Manuscript is fully protected by copyright and cannot be reused or reposted elsewhere.

As the Version of Record of this article is going to be / has been published on a subscription basis, this Accepted Manuscript is available for reuse under a CC BY-NC-ND 3.0 licence after the 12 month embargo period.

After the embargo period, everyone is permitted to use copy and redistribute this article for non-commercial purposes only, provided that they adhere to all the terms of the licence <https://creativecommons.org/licenses/by-nc-nd/3.0>

Although reasonable endeavours have been taken to obtain all necessary permissions from third parties to include their copyrighted content within this article, their full citation and copyright line may not be present in this Accepted Manuscript version. Before using any content from this article, please refer to the Version of Record on IOPscience once published for full citation and copyright details, as permissions will likely be required. All third party content is fully copyright protected, unless specifically stated otherwise in the figure caption in the Version of Record.

View the [article online](#) for updates and enhancements.

1 Fabrication, characterisation and analytical modelling of gradient auxetic closed cell 2 foams

3 **Olly Duncan^{1*}, Andrew Alderson², Tom Allen¹**

4 ¹ *Department of Engineering, Faculty of Science & Engineering, Manchester Metropolitan University, John
5 Dalton Building, Chester Street, Manchester M1 5GD, UK.*

6 ² *Materials and Engineering Research Institute, Faculty of Science, Technology and Arts, Sheffield Hallam
7 University, Howard Street, Sheffield S1 1WB UK.*

8 * Corresponding author (Email: O.Duncan@mmu.ac.uk)

9 **Abstract**

10 Auxetic (negative Poisson's ratio) and gradient open cell foams have shown promise for their
11 conformability and high impact energy absorption – useful in applications like protective
12 equipment, footwear and prosthetics. Recent methods fabricated closed cell auxetic foam by
13 steaming conventional closed cell foam. Methods developed herein control the cell structure
14 of auxetic closed cell foam, to produce novel intentionally anisotropic and gradient auxetic
15 closed cell foam. Pins passed through the foam constrained or stretched regions during
16 steaming to further modify cell structure and impart gradients in cell structure, Young's
17 modulus and Poisson's ratios. Fabricated foams had Poisson's ratios between 1 and -1.
18 Imparted Young's moduli of 1 to 12 MPa were similar to foams used in footwear, prosthesis,
19 helmets and other impact protection. The effect of changes to cell structure on Young's moduli
20 and Poisson's ratio are explained by combining analytical models of auxetic open cell and
21 conventional closed cell foam.

22 **Keywords**

23 negative Poisson's ratio, gradient, foam, impact protection, steam processing

24 **1. Introduction**

25 Auxetic foam has a negative Poisson's ratio (NPR; expanding transversely when stretched
26 and contracting transversely when compressed) [1]. NPR can increase conformability [2,3],
27 indentation resistance [4,5], impact energy absorption [6–8], vibration damping [9–11], acoustic
28 [12–14] and thermal insulation [15,16] and shear modulus [17,18], while also causing biaxial
29 expansion and domed curvature [19,20]. Auxetic open cell foams, with established fabrication
30

1
2
3 30 methods [1,21,22], have been proposed and tested for a range of applications, including in
4
5 31 prosthetic devices [19,23], seating [24], footwear [25], vibration limiting gloves for use in
6
7 32 construction [11], crash barriers and pads [24,26], sports helmets [27] and other personal
8
9 33 protective equipment [8,26,28]. Most auxetic foam research focusses on open cell foam with
10
11 34 Young's modulus below ~ 0.2 MPa [29,30]. A recent study produced low porosity open cell
12
13 35 foam sheets with planar NPR in tension, and through thickness Young's moduli up to 25 MPa
14
15 36 [31]. Personal protective equipment generally uses porous closed cell foam, containing trapped
16
17 37 gas or air to increase the stiffness provided by the foam cell structure to between 1 and 20 MPa
18
19 38 [32–34]. Without established methods to fabricate porous auxetic foams with desirable
20
21 39 stiffness, products containing auxetic foams are not common.

22
23
24
25
26 40 Typical auxetic open cell foam fabrications first compress conventional thermo-plastic
27
28 41 open cell foam, buckling cell ribs to impart a re-entrant like cell structure, which is commonly
29
30 42 associated with NPR [1,21,22]. Heating and cooling cycles can then fix the imposed structure
31
32 43 over time, so these fabrications are known as thermo-mechanical fabrications [1,21,35].
33
34 44 Solvents or gases can also be used as softening agents [22,36,37]. Anisotropic auxetic open
35
36 45 cell foams can be made by applying different levels of compression in different directions
37
38 46 [6,31,38]. Thermo-forming with curved moulds can also produce curved auxetic open cell foam
39
40 47 [39]. Thermo-forming recently produced foam sheets with tensile NPR in both planar
41
42 48 directions. The foam was highly compressed through thickness during thermo-forming,
43
44 49 reducing through thickness porosity while imparting Young's modulus up to 25 MPa and
45
46 50 positive compressive Poisson's ratio [31].

47
48
49
50
51 51 Gradient foams have different cell structures, Young's moduli and Poisson's ratio in
52
53 52 pre-defined regions, and gradients can be discrete or continuous [19,23,40]. During open cell
54
55 53 auxetic gradient foam fabrications, compression can be controlled, and hence varied, by
56
57 54 passing pins through the foam sample, or by using a foam sample with a different shape to the
58
59
60

1
2
3 55 mould [19,23,40]. Applying different compression regimes to different foam regions during
4
5 56 fabrication can produce gradient open cell auxetic foams. Stretching foams in one or more
6
7 57 directions by passing pins through the foam during fabrication produces long, re-entrant cells,
8
9 58 increasing Young's modulus and the magnitude of positive or negative Poisson's ratio during
10
11 59 loading parallel to the long cell axis [38,40,41]. Foam in personal protective equipment is often
12
13 60 segmented so it fits the body better than a continuous sheet [42–44], but any reduction or loss
14
15 61 of padding between segments may reduce protection. Varying material properties in running
16
17 62 shoe midsole regions can influence and improve running style [45]. Gradient foams may offer
18
19 63 benefits to personal protective equipment and footwear in terms of how they comfortably
20
21 64 cover, deform with and protect body segments [19,23,40].

22
23
24
25
26 65 Chan and Evans found thermo-mechanical fabrications to rupture closed cell foam
27
28 66 walls during fabrication [21,46]. Fabrication methods for auxetic closed cell foams that do not
29
30 67 rupture cells use hydrostatic compressive pressure applied by a pressure vessel [47], or steam
31
32 68 absorption and condensation [48,49]. Cell structure, Poisson's ratio and Young's moduli of
33
34 69 closed cell auxetic foams vary with compression imparted following fabrication, with common
35
36 70 volumetric compression ratios (original/final volume) being between 1.3 and 6.0 [47–49]. Of
37
38 71 the two available options for fabricating closed cell auxetic foam, the steam fabrication method
39
40 72 uses simpler equipment, such as a steam bath or an oven and a water filled container [48,49].
41
42 73 Upon cooling, as the foam shrinks and cell walls become re-entrant, the constituent polymer in
43
44 74 some foams, such as polyethylene, passes through a thermal transition that fixes the imposed
45
46 75 cell structure [48,49]. Absorbed water can, then, evaporate from the foam within a week of
47
48 76 fabrication, leaving a stable auxetic closed cell foam with negligible trapped water [48,49].
49
50
51
52

53
54 77 Auxetic and conventional closed cell foam characteristics have been explained using
55
56 78 dimensions estimated from two-dimensional (2D) projections of cell structures, based on
57
58 79 microscopic imaging. Analytical models for conventional and auxetic foam consider the
59
60

1
2
3 80 stretching, flexing and hinging of cell ribs to predict Poisson's ratios and Young's moduli
4
5 81 [40,41,50]. No analytical model has been published considering infrequently researched
6
7 82 auxetic closed cell foams. Analytical models for conventional closed cell foams have combined
8
9 83 the effects of gas pressure on cell rib and wall deformation, estimating dimensions and
10
11 84 orientations from 2D cell projections [41,51,52].
12
13

14 85 Auxetic closed cell foam fabrications that rely solely on pressure differentials offer
15
16 86 limited control over compression [47–49]. As such, before beginning a study fabricating a new
17
18 87 type, size or shape of auxetic closed cell foam, pilot work is needed to find the processing
19
20 88 conditions that give the desired volumetric compression. Gradient or intentionally anisotropic
21
22 89 auxetic closed cell foams have not previously been produced. This work explores two steam
23
24 90 fabrication-based methods to control cell structure modification in different axis and foam
25
26 91 regions. These fabrication methods were: i) Constraining or stretching foam regions, using
27
28 92 pins, to produce intentionally anisotropic gradient foam, and ii) Preventing steam from
29
30 93 reaching regions of a sample, to produce gradient foam. The effect of these methods and
31
32 94 modifications to cell structure, on Young's modulus and Poisson's ratio, are explained by
33
34 95 combining analytical models for open cell auxetic foam [40] and the effect of gas pressure in
35
36 96 closed cell foam [51,52].
37
38
39
40
41
42

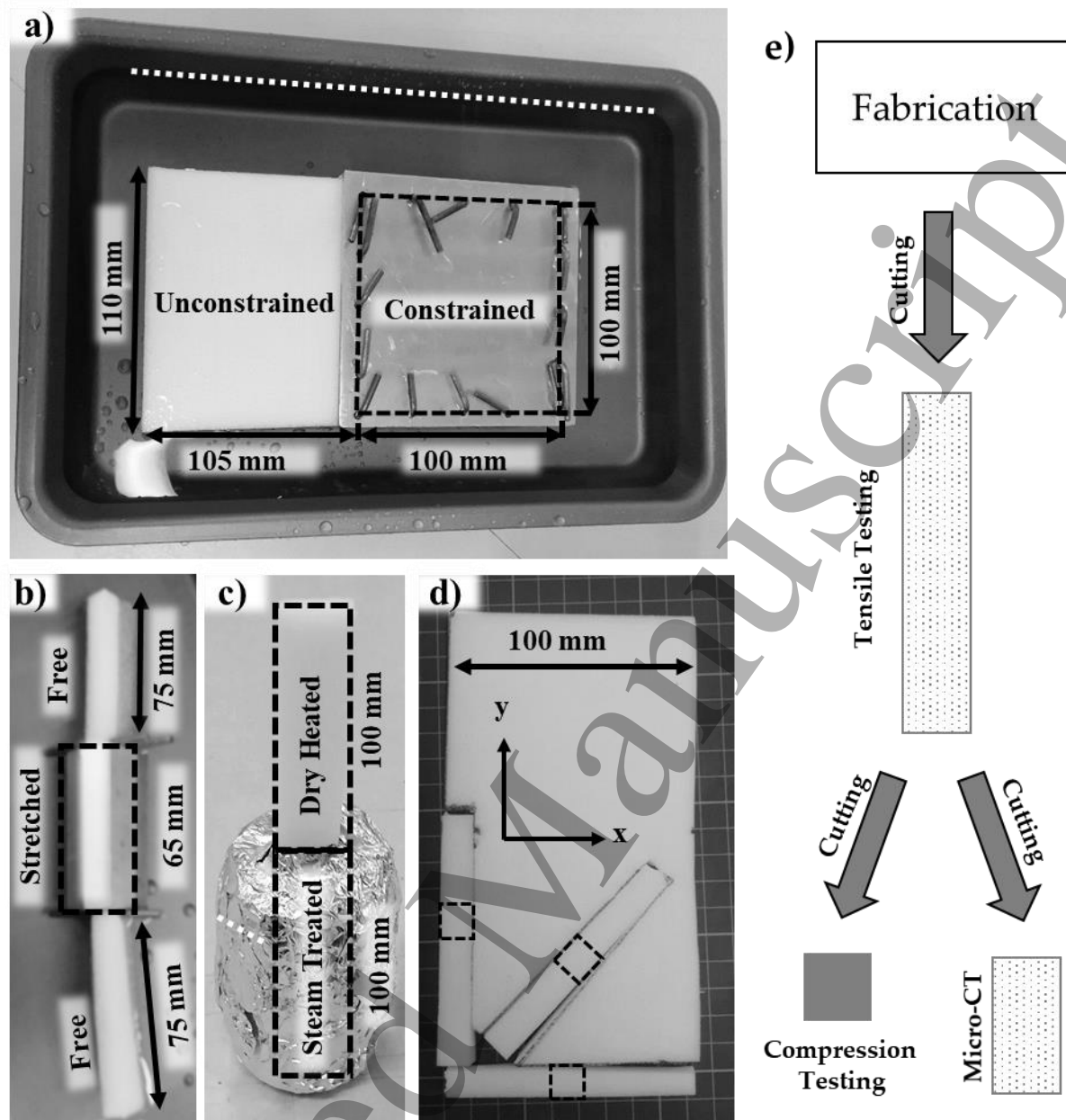
43 97 **2. Methods**

44 98 **2.1. Fabrication**

45 99 Two sheets (210 × 110 × 10 mm) and two cuboids (200 × 20 × 10 mm) of closed cell foam
46
47 100 (Plastazote LD-60, algeos.com), pre-conditioned for a week in an environmental chamber
48
49 101 (20°C and 10% relative humidity), were fabricated by steam processing [48,49]. One sheet of
50
51 102 foam was unconstrained during fabrication. The other sheet was constrained at one end by
52
53 103 twelve steel pins (Ø2 mm) passed through holes in aluminium plates (100 × 100 × 2 mm),
54
55 104 sandwiching but not compressing the foam (Figure 1a). Pins were inserted in each corner and
56
57
58
59
60

1
2
3 105 along each side of the plates with 33 mm spacing. The central 45 mm of one cuboid (i) was
4
5 106 stretched to 1.5 times its original length, using four pins passed through the foam and an
6
7 107 aluminium box section (surrounding but not touching) to hold the pins apart (2 mm thick walls,
8
9
10 108 $22 \times 22 \times 65$ mm Figure 1b). Foam samples and constraining devices were placed in 250×350
11
12 109 $\times 40$ mm aluminium dishes (2 mm thick walls) filled to ~ 30 mm with water and covered with
13
14 110 aluminium foil [49]. Cuboid (ii) was positioned with half its length inside an aluminium drinks
15
16 111 can ($\text{\O}70$ mm, height 100 mm, 1 mm wall thickness), filled to 80% with water, and with a ~ 15
17
18 112 $\times 15$ mm hole in the top. The foam was passed through the hole in the can, so the upper half
19
20 113 was dry heated during fabrication (Figure 1c).
21
22
23

24 114 All containers were heated in an oven (MCP Tooling Technologies LC/CD, $\pm 0.25^\circ\text{C}$) set
25
26 115 to 105°C for 4.5 hours [49]. After steaming, samples and constraining devices were removed
27
28 116 from the containers and cooled for 30 minutes on a drying rack in an air-conditioned laboratory
29
30 117 with an expected temperature of 20 to 25°C and relative humidity of 30 to 60%. Samples began
31
32 118 to shrink upon removal from the water, with shrinking appearing to finish within 1 to 2 minutes.
33
34 119 Constraining devices were then removed, and samples were returned to the environmental
35
36 120 chamber for a week before testing. The order of cutting (Figure 1d), and testing, is shown in
37
38 121 Figure 1e (tensile tests, then compression tests or micro-ct). Samples were returned to the
39
40 122 environmental chamber between tests. Tests were in the air-conditioned laboratory described
41
42 123 above (20 to 25°C and relative humidity of 30 to 60%).
43
44
45
46
47
48
49
50
51
52
53
54
55
56
57
58
59
60



124

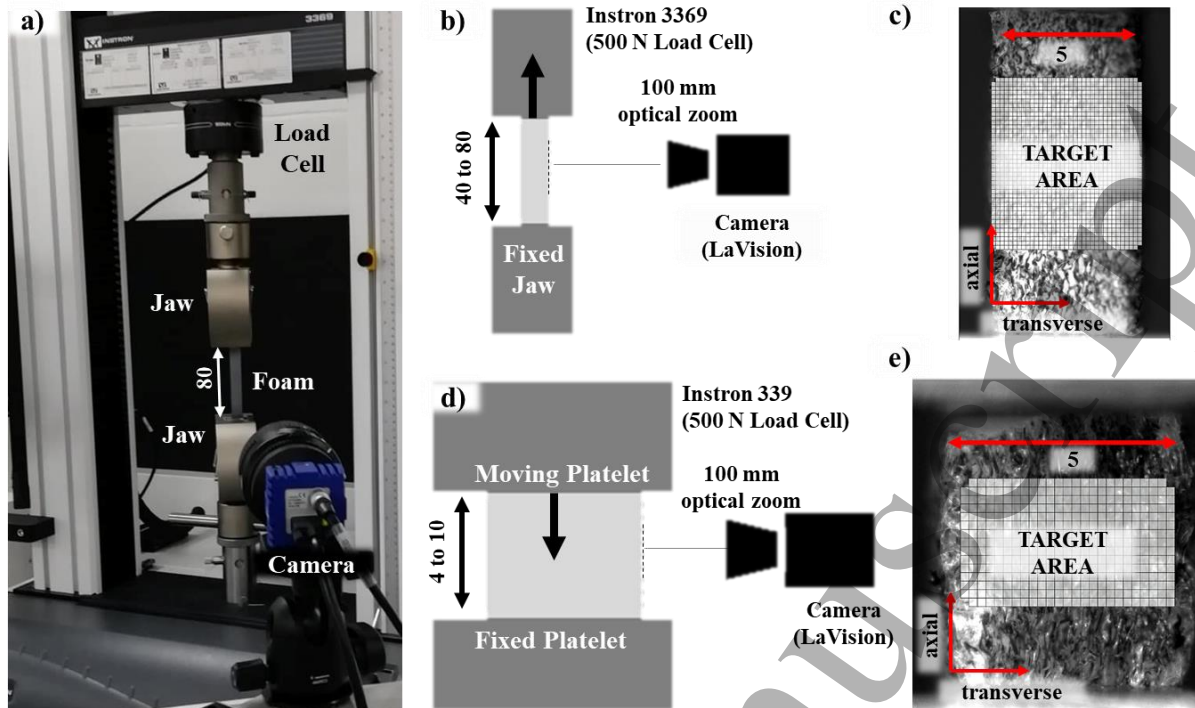
125 **Figure 1.** a) Sample containing constrained region (note the 5 mm edge surrounding the constrained region); b)
 126 Sample containing stretched region; c) Sample half steamed and half dry heated; d) Example tensile cuboids and
 127 compression (dashed lines) with sample orientations, locations and axis labelling marked; e) Order of sample
 128 preparation. The same orientations and co-ordinate systems were used for all sheets/regions. Y-axis parallel to
 129 sample length, x to width in (b) and (c). White dotted lines in (a) and (c) show water level.

130 2.2. Characterisation

131 Mass (Sartorius, M-power) and dimensions (Vernier Calipers) of all samples and
 132 regions were measured before and one week after fabrication, to see if any cells contained
 133 water, which would increase mass, and to measure linear compression ratios in each orthogonal
 134 axis (LCR, final/original length). The partially open cells on the faces of foam samples do not

1
2
3 135 shrink during fabrication as they cannot trap steam [48,49]. Therefore, 1 to 2 mm was cut from
4
5 136 the planar edges of converted samples with a utility knife (Stanley) before characterisation.
6
7 137 The top and bottom faces were not removed, as samples were already thin (3 to 5 mm). Three
8
9 138 samples of unconverted foam ($100 \times 10 \times 10$ mm), foam from the unconstrained sheet and
10
11 139 from each region of the gradient sheet ($\sim 60 \times 5 \times 5$ mm) were cut for tensile tests, with the
12
13 140 utility knife, at 45° increments (Figure 1d). The two cuboids were cut for tensile testing, with
14
15 141 one $\sim 60 \times 5 \times 5$ mm sample taken from each region (three samples in Figures 1b and two in
16
17 142 c). The dimensions and mass of the tensile samples were used to calculate final density ratio
18
19 143 (FDR, final/original density).
20
21
22
23

24 144 A speckle pattern was applied to all samples (matt Acrylic spray paint, Halfords) for
25
26 145 full-field strain measurement using 2D digital image correlation (DIC). Tensile tests were at a
27
28 146 strain rate of 0.0033 s^{-1} to 10% tension on an Instron 3369 with a 500 N load cell sampling at
29
30 147 25 Hz. Samples were clamped ~ 10 mm from their ends in the jaws of the device, which were
31
32 148 closed to 1 mm, giving gauge lengths of 40 to 80 mm. These cuboidal samples had longer
33
34 149 gauge lengths (>35 mm) and were thinner than the 12 mm sided ‘dog-bone’ samples specified
35
36 150 in ASTM D3574 – 11, to account for end effects [53]. Tensile tests were filmed with a camera
37
38 151 (**Figure 2a**), with its image plane aligned to a face of the sample (LaVision DIC package, 1260
39
40 152 $\times 1080$ p, 10 fps, Nikon lenses with 100 mm optical zoom). A target area was defined over the
41
42 153 central lengthwise third of samples (Figure 2b & c), giving axial and transverse true strains,
43
44 154 with facet sizes set to give at least three speckles per facet (10 to 15 pixels) [54]. Device jaws
45
46 155 were rotated 90° around the loading axis between tests, with the sample in place, to apply strain
47
48 156 mapping to four faces. Sample cross sectional areas were measured before each test with
49
50 157 Vernier Calipers to allow stress to be calculated.
51
52
53
54
55
56
57
58
59
60



158
159 **Figure 2.** a) Tensile sample and camera, b) Tensile test schematic; c) tensile sample with speckle pattern and
160 target area; d) compression test schematic; e) compression tests sample with speckle pattern and target area.
161 Dimensions in mm.

162 Cubes for compression testing (4 to 10 mm sided) were cut from the lengthwise centre
163 of all tensile samples one day after testing, and dimensions were measured (Figure 1d). These
164 cubes were smaller than specified in ASTM D3574 – 11 due to the low initial foam thickness
165 [53]. Three cubes were cut from the stretched region of the gradient cuboid in Figure 1b to
166 allow repeat testing of the only foam that was stretched during fabrication. Cubes were
167 compression tested in all three orthogonal axes between platelets using the same equipment
168 and settings as the tensile tests (Figure 2d & e) and a preload of 0.1 N to ensure contact,
169 corresponding to 0.25 to 0.75% compression. Incremental Poisson's ratios were calculated by
170 fitting linear trend lines to transverse vs. axial engineering strain data (from DIC, same system
171 as tensile tests) at 0.5 or 1% axial strain increments, depending on the number of available data
172 points for regression fitting. Incremental tangent moduli were calculated in the same way, from
173 stress vs. axial engineering strain data from Instron's software Bluehill 4.0's force and

1
2
3 174 displacement, and measured sample dimensions. Young's moduli were taken as the tangent
4
5 175 moduli at the lowest calculated axial strain (up to 0.5 or 1%).
6
7

8 176 To see cell shapes, micro-computed tomographic (micro-ct) scans of $\sim 5 \times 5 \times 20$ mm
9
10 177 samples from each region of each type of foam were collected (SkyScan 1172; 360° rotation,
11
12 178 image acquisition every 1.4°, resolution $< 5 \mu\text{m}$). Micro-ct data were rendered (SkyScan,
13
14 179 CTVox) and images taken of one cell (~ 100 to $500 \mu\text{m}$) deep volumes in each orthogonal axis.
15
16 180 To help compare cell structures, single cell images were processed by removing unconnected
17
18 181 pixels with areas under 2% of the cell using erosion functions (*imclose* and *bwareaeopen*) in
19
20 182 MATLAB® 2019a (Mathworks, USA).
21
22
23

24 183 **2.3. Analytical Modelling**

25
26 184 Analytical models based on 2D cell projections [40], and the effect of air pressure based
27
28 185 on analysis of the same polyethylene foam of lower density (LD-24, Zotefoam) [51], were
29
30 186 combined and adapted. The adapted model was used to explain Young's moduli (E_y and E_z)
31
32 187 and Poisson's ratios (ν_{yz} and ν_{zy}) at 0.75% compression and tension (ϵ_y and ϵ_z). The value of \pm
33
34 188 0.75% strain was selected as the 2nd data point in most Tangent moduli and Poisson's ratio vs.
35
36 189 strain data. Details of the model for 2D cell projections, taken from previous open cell foam
37
38 190 work [40], are included as Supplementary Material S2, with unitless dimensions relative to the
39
40 191 vertical rib length ($h = 1$, which is diagonal rib length). Some changes to cell dimensions were
41
42 192 made from the previous study [40]. As low cell wall thickness is common in closed cell foams
43
44 193 [41,51], relative rib/wall thickness was halved from 0.2, as used in the previous open cell foam
45
46 194 work [40], to 0.1 (Figure S6). Cell walls were partially constrained by gas pressure; increasing
47
48 195 the relative amount of stretching, rather than flexure and hinging, as discussed elsewhere [51].
49
50 196 With the support from the internal air pressure, rather than reducing the flexure and hinging
51
52 197 constant (k_{hf}) for the thinner walls, k_{hf} was increased from 0.04 [40] to 0.10 in tension. Cell
53
54 198 walls of unconverted closed cell foam begin to buckle at low (0 to 3%) compression [51]. Since
55
56
57
58
59
60

199 many of the converted foams had kinked cell walls from fabrication, buckling was expected to
 200 occur at close to 0% compression, so k_{hf} was reduced three-fold (to 0.03) in compression, which
 201 was an arbitrary amount found to fit the data. Sensitivity to variations in k_{hf} are shown in the
 202 supplementary material (Figure S5). The force constants for flexing and hinging were
 203 unchanged from the previous model (0.04 and 0.0044, respectively) [40]. To account for gas
 204 pressure, relative volumetric deformation (Equation 1) was [51,52]:

$$\varepsilon_v = \frac{\varepsilon_u}{(1-\varepsilon_u-R)} \quad (1)$$

206 where relative density (R) was the density of polyethylene (~900 kg/m³ [51]) divided by the
 207 measured foam density, and ε_v and ε_u were volumetric and uniaxial strains, respectively. The
 208 contribution of air pressure (p_{air}) to Young's modulus (E_{air} , Equation 2) was [51]:

$$E_{air} = \frac{p_{air}}{\varepsilon_u} = \frac{\varepsilon_v * p_0 * (1-2\nu)}{\varepsilon_u} \quad (2)$$

210 where p_0 was air pressure inside cells before testing, which was assumed to be atmospheric
 211 pressure (100 kPa) [51]. The foam modulus ($E_{combined}$) was calculated by adding the gas
 212 pressure contribution from Equation (2) and cellular modulus (E_{cell}) from Equation (S5) [51].

$$E_{combined} = E_{PE} * E_{cell} + E_{air} \quad (3)$$

214 where E_{PE} was the Young's modulus of polyethylene (300 MPa) [51]. Values for E_y and E_z
 215 were normalised to E_y from the analytical model at 0% strain and multiplied by the mean of
 216 measured compressive and tensile E_y . The combined Poisson's ratio ($\nu_{combined}$) was:

$$\nu_{combined} = \nu_{cell} + \nu_{fluid} * \frac{E_{air}}{E_{trans-cell}} \quad (4)$$

218 where ν_{cell} was the cellular Poisson's ratio contribution (ν_{cell} , Equation S6), ν_{fluid} was the
 219 Poisson's ratio of a fluid (of 0.5) and $E_{trans-cell}$ was the cellular transverse Young's modulus.
 220 Estimating the effect of trapped gas on Young's modulus and Poisson's ratio, rather than
 221 calculating its effect on cell rib deflection, means this analytical model can only show trends
 222 at low strains (< 1%).

223 3. Results

224 3.1 Sample measurements

225 Foam density increased (from $50.2 \pm 0.8 \text{ kg/m}^3$, mean \pm standard deviation (S.D.)) for
226 the steamed samples following fabrication, giving FDRs between ~ 3 and 4 (**Figure 3a**).
227 Density was unchanged (FDR = 1.0) for the dry heated region of foam that was not exposed to
228 steam (in Figure 1c). Change in mass after a week in ambient conditions, before any other
229 testing, was negligible (up to 0.3%), indicating any trapped water had evaporated and any
230 increase in sample density was likely due to a decrease in volume. Unconstrained regions (FDR
231 between 3.5 and 4.0) shrank more after fabrication than constrained regions (FDR between 3.0
232 and 3.5).

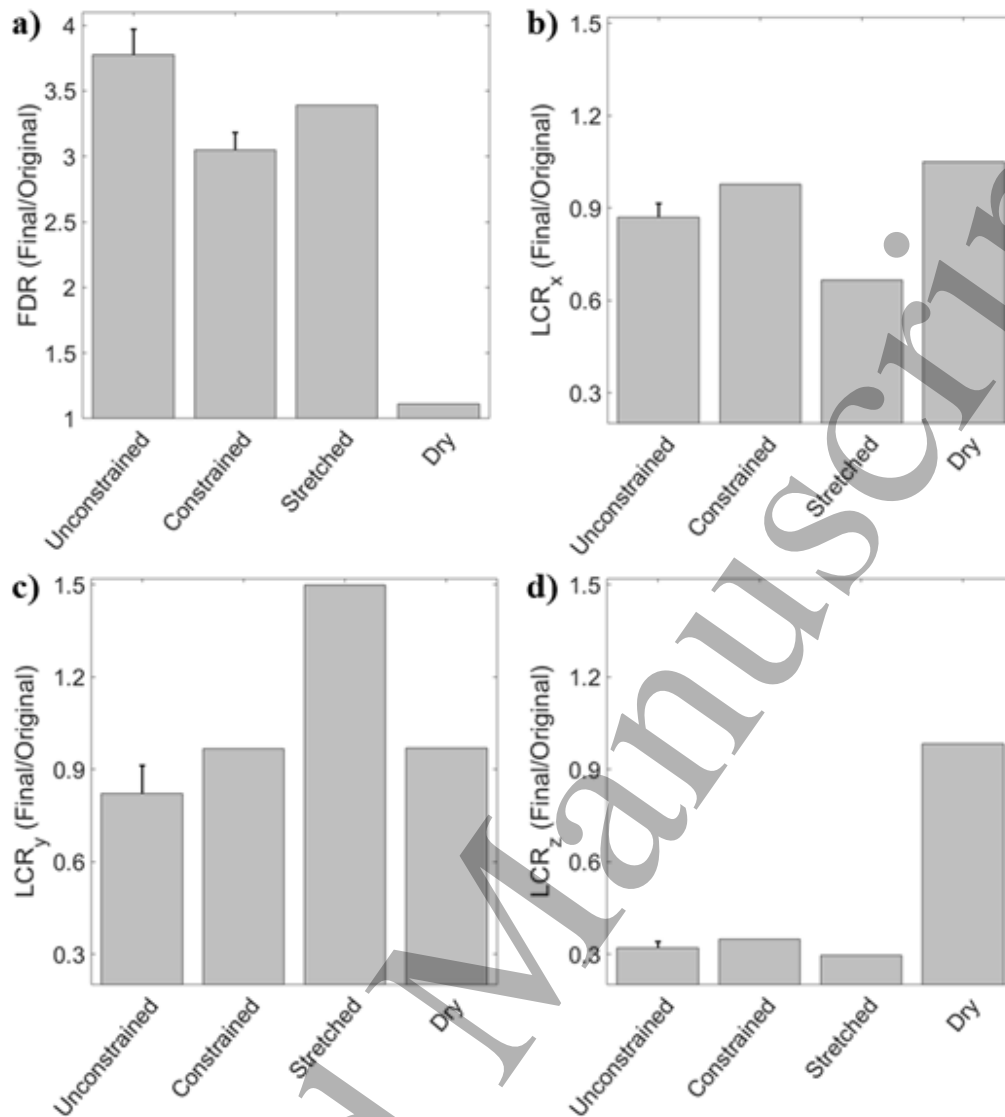


Figure 3. a) Final density ratio of samples cut for tensile testing and; b) to d) linear compression ratios measured from whole processed samples, parallel to the b) x-axis (shorter side), c) y-axis (longer side), and d) z-axis (through thickness). Same legend (d) for all. Error bars show 1 S.D. for conditions where multiple samples were fabricated.

Considering the unconstrained, steamed foam samples and regions, planar (x and y) LCRs (Figure 3b & c) were about 0.9, with more through thickness shrinking (LCR_z ≈ 0.3, Figure 3d). The constrained region of the gradient sheet exhibited planar LCRs of 1.0 (i.e. unchanged, due to the constraints) and an LCR of 0.3 through thickness. The stretched region of the steamed cuboid retained its applied LCR of ~1.5 in its y-axis (Figure 3c), an LCR of 0.7 in the x-axis (Figure 3b) and similar through thickness LCR to other samples (LCR_z ≈ 0.3, Figure 3d).

3.2 Cell Structures

There was negligible difference in cell structure between orientations for the unconverted foam (**Figure 4a to c**), suggesting little to no elongated cell rise [41], as expected [49]. Steam contraction in the unconstrained sheet (**Figure 4d & e**) reduced cell size and imparted different topology, corresponding to some kinks in the previously straight cell walls, which were most obvious through thickness (**Figure 4d**). The structure of cells on the outer faces of samples barely changed following fabrication, as cells on the outer faces were partially open from cutting and could not trap steam (**Figure 4f**). Constraining foam in two directions created a similar effect to the unconstrained conversion, except the cells were wide, with low thickness (**Figure 4g**), but similar to the unconverted foam (**Figure 4a to c**) in the constrained x-y plane (**Figure 4h**) and on their outer faces (**Figure 4i**). Stretching foam in the y-axis also produced a similar effect, with wider, thinner cells still (**Figure 4g**), and different topology, corresponding to some kinked cell walls in the x-y plane (**Figure 4k**), caused by contraction in the x-axis ($LCR_x = 0.7$, **Figure 3b**). The outer faces of steamed samples had hexagonal cells, which were longer in their stretched y-axis for samples stretched by pins during fabrication (**Figure 4l**).

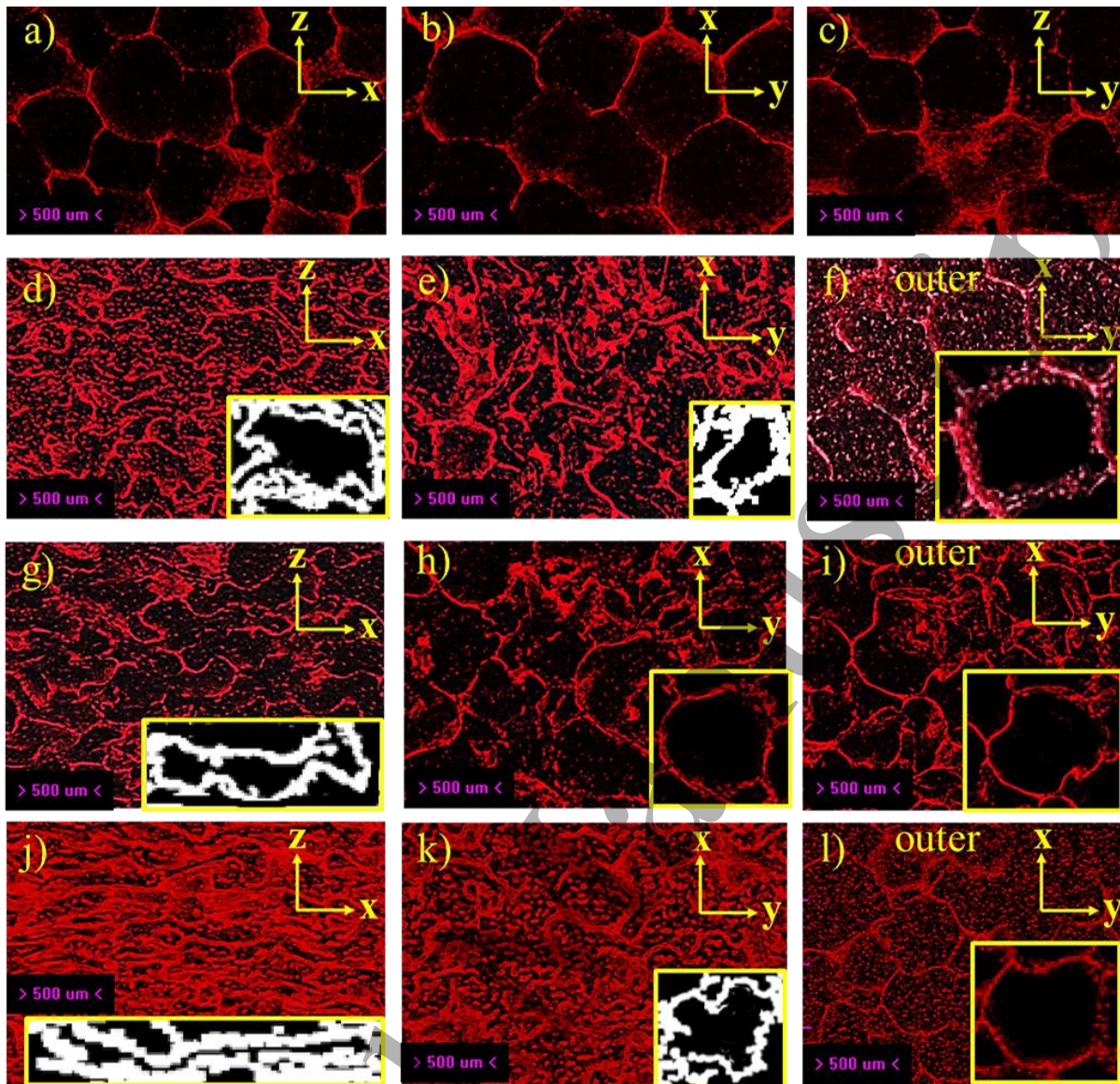
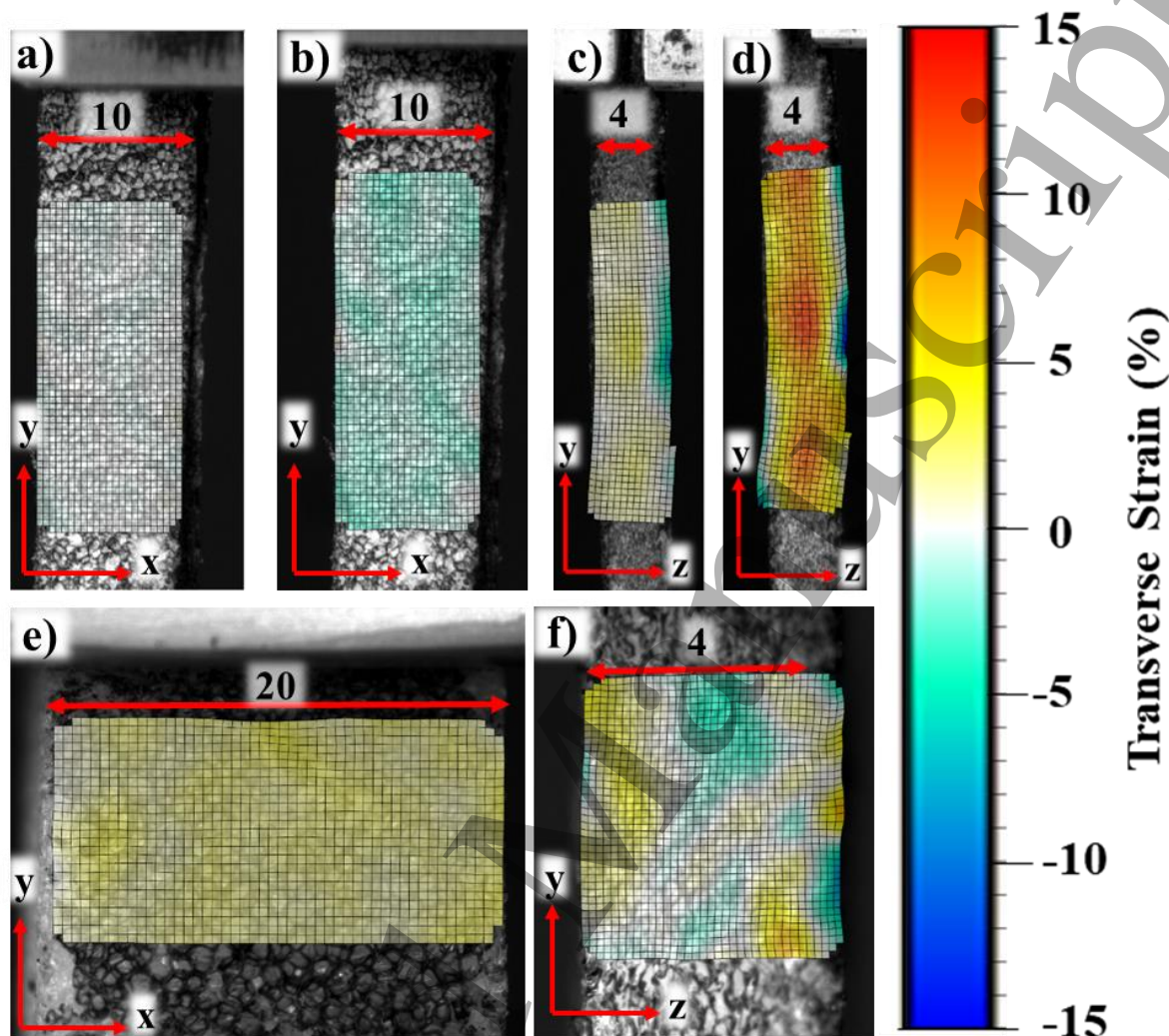


Figure 4. Micro-ct scans of a) to c) unconverted foam; d) to f) unconstrained, steamed sheet sample, g) to i) the constrained region of the constrained sheet, j) to l) the stretched region of the partially stretched gradient cuboid. Labels show orientation, subfigures f), i) and l) show steamed foam's outer face. Inserts in d) to l) show processed single cell images digitally expanded by 1.5 times their original size. White single cell images were processed in MATLAB®, others by minor manual editing to accentuate cell walls.

3.3 Digital Image Correlation

Contour plots of transverse strain from DIC show the unconverted foam contracted transversely at 2 and 10% tension (**Figure 5a & b**) and the auxetic foam expanded (Figure 5c & d). Contour plots at 10% compression show the unconverted foam expanded transversely (Figure 5e). The auxetic sample contracted transversely at the centre (Figure 5f) and expanded along the edges; corresponding to regions with (Figure 4g) and without (Figure 4i) re-entrant

273 cell structures, respectively. See supplementary video for strain mapping of uniform and
 274 gradient samples in tension.

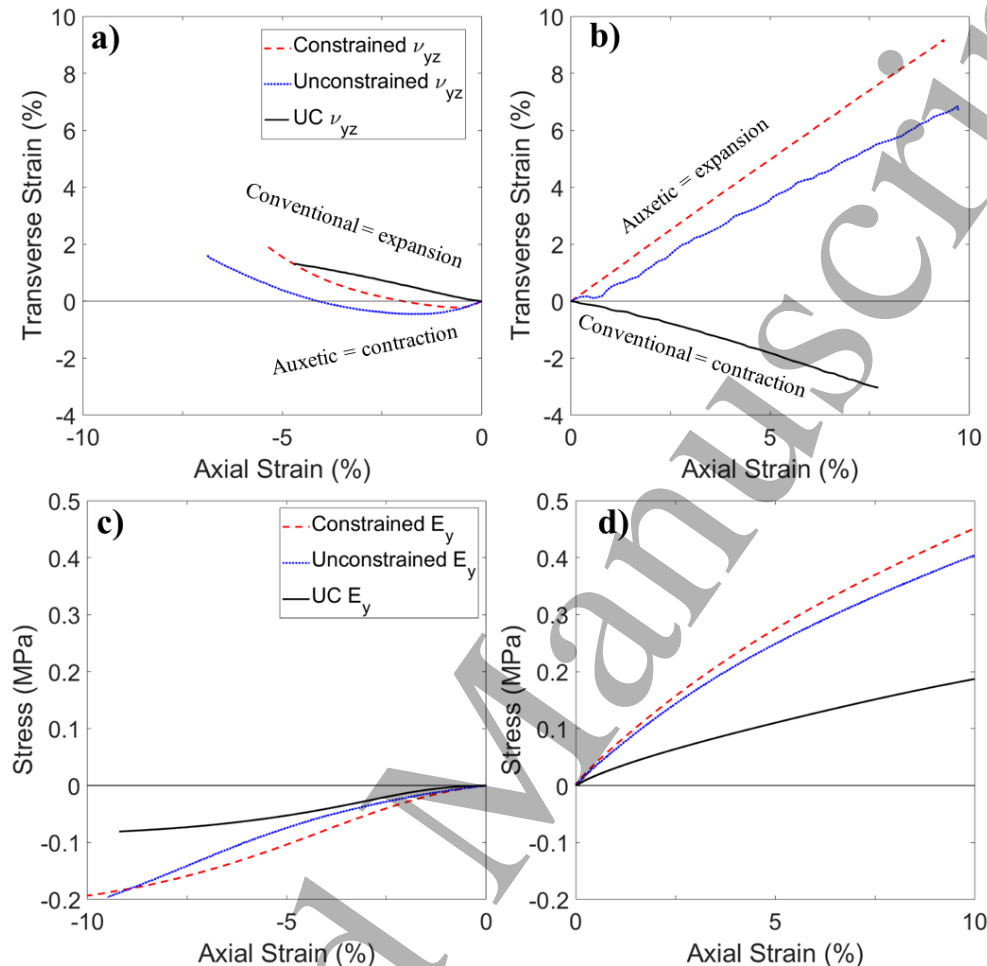


275 **Figure 5.** Contour plots of transverse strain from DIC of a) and b) unconverted foam at a) 2% and b) 10% tension;
 276 c) and d) the constrained region of the gradient sheet at c) 2% and d) 10% tension; e) unconverted foam at 10%
 277 compression; f) the constrained region of the gradient sheet at 10% compression. Labelled dimensions are in mm.
 278

279 3.4 Stress and lateral strain vs. axial strain

280 NPR behavior (i.e. contraction) of the unconstrained foam was retained to ~2 to 3%
 281 compression (**Figure 6a**), followed by transverse expansion. The constrained region of the
 282 gradient sheet had a steeper compressive axial vs. transverse strain relationship and therefore
 283 a higher magnitude of (negative) Poisson's ratio than the unconstrained region. NPR was,
 284 however, only maintained to ~1% compression in the constrained region. Tensile transverse
 285 vs. axial strain was quasi-linear for all samples (**Figure 6b**), with the constrained region of the
 286

286 gradient sheet expanding more transversely than the unconstrained region. The unconverted
 287 foam exhibited transverse expansion in compression (Figure 6a) and transverse contraction
 288 (Figure 6b) in tension.



289 **Figure 6.** Sample plots of a) & b) Transverse vs. axial strain in a) compression and b) tension; c) & d) Stress vs.
 290 axial strain for constrained and unconstrained regions of the gradient sheet, and the unconverted foam in c)
 291 compression and d) tension. Negative strain values indicate axial compression and transverse contraction. Same
 292 legend applies to a) & b), and c) & d).
 293

294 The unconverted foam exhibited its characteristic stress vs. strain plateau at ~5%
 295 compression [41,49,55] (Figure 6c). The constrained region of the gradient sheet also had a
 296 stress vs. strain plateau, at ~8% compression, and a steeper initial gradient and therefore higher
 297 Young's modulus than both the unconverted and unconstrained regions. The unconstrained
 298 region exhibited linear stress vs. strain of steeper gradient than the unconverted foam. In
 299 tension (Figure 6d), stress vs. strain relationships of all samples were quasi-linear, with the

1
2
3 300 same order of low to high Young's moduli as in compression (unconverted < unconstrained <
4
5 301 constrained).

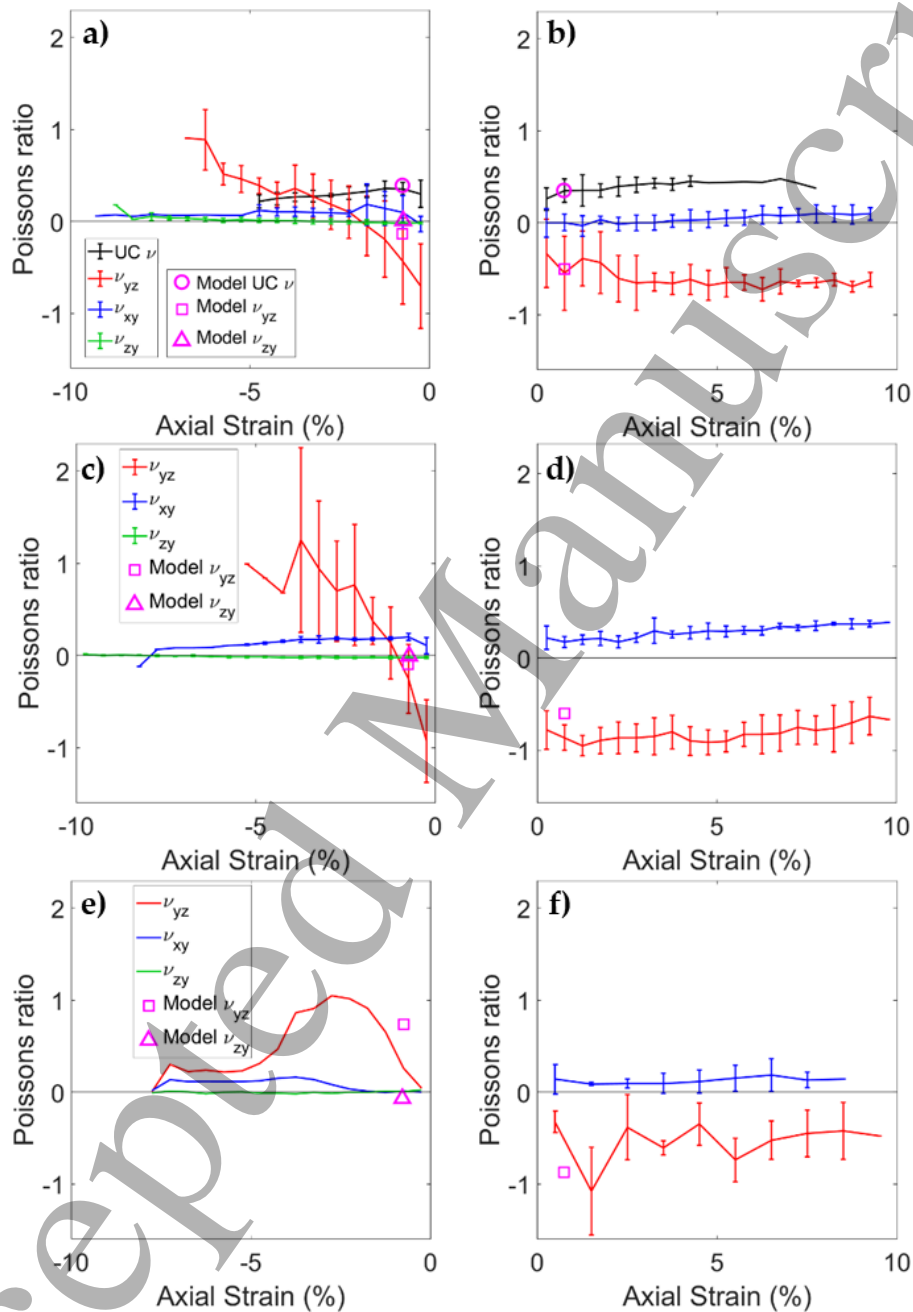
8 302 **3.5 Poisson's ratios**

9
10 303 The unconverted sample was isotropic ($\nu \approx 0.4$, **Figure 7a & b**, Supplementary Material
11 304 S1). Measured Poisson's ratios and tangent moduli of test samples cut from unconstrained
12 305 regions of different fabricated samples were similar to each other (Figures S1 & S2). A
13 306 selection of samples, from the constrained and stretched regions of gradient foams,
14 307 demonstrating the different mechanical behaviors and imparted cell structures are outlined
15 308 here. Detailed results are included in the supplementary material (Figures S1 & S2), along with
16 309 collated Young's modulus and Poisson's ratio data (Supplementary Table S1). The mechanical
17 310 properties of the dry heated region of foam were similar to the unconverted foam (Figures S1
18 311 & S2), as FDR and LCRs were ≈ 1 , so cell structures were unchanged (Figure 3).

19 312 Concerning the gradient sheet, tensile and low strain (<0.5%) compressive Poisson's
20 313 ratios of the unconstrained section were as low as -0.7 (ν_{yz} , Figure 7a & b). In the slightly
21 314 compressed in-plane directions (LCR ≈ 0.9), Poisson's ratios ($\nu_{xy} \approx 0.1$) were lower than for
22 315 the unconverted foam. During through thickness compression tests, ν_{zy} was about zero. In the
23 316 unconstrained foam section (Figure 7c & d), Poisson's ratio had greater anisotropy; NPR
24 317 reached a higher magnitude ($\nu_{yz} \approx -1.0$), whereas the in-plane Poisson's ratio was closer to that
25 318 of the unconverted foam ($\nu_{xy} \approx 0.2$). Through thickness compressive Poisson's ratio (ν_{zy}) was
26 319 also close to zero (Figure 7c). Trends in the stretched region (Figure 7e & f) were broadly
27 320 similar to the constrained region, but the positive Poisson's ratio ν_{yz} (of 1) was higher in
28 321 compression; as in similar work stretching open cell foam during fabrication [38,40].

29 322 Calculated Poisson's ratios, based on Equation (4) and schematics in Supplementary
30 323 Figure S3, show reasonable agreement (within ~ 1 S.D.) with measured values (Figure 7 &
31 324 Supplementary Material S2). The analytical model predicts that the effect of transverse

325 expansion of gas in compression increases with cell anisotropy (Supplementary materials
 326 Figure S4 -S8), as does Figure 7 data. NPR (ν_{yz}) was present up to 2 to 3% compression for the
 327 unconstrained region (Figure 7a) and 1 to 2% for the constrained region (Figure 7c), whereas
 328 the stretched foam had positive compressive Poisson's ratio (Figure 7e).

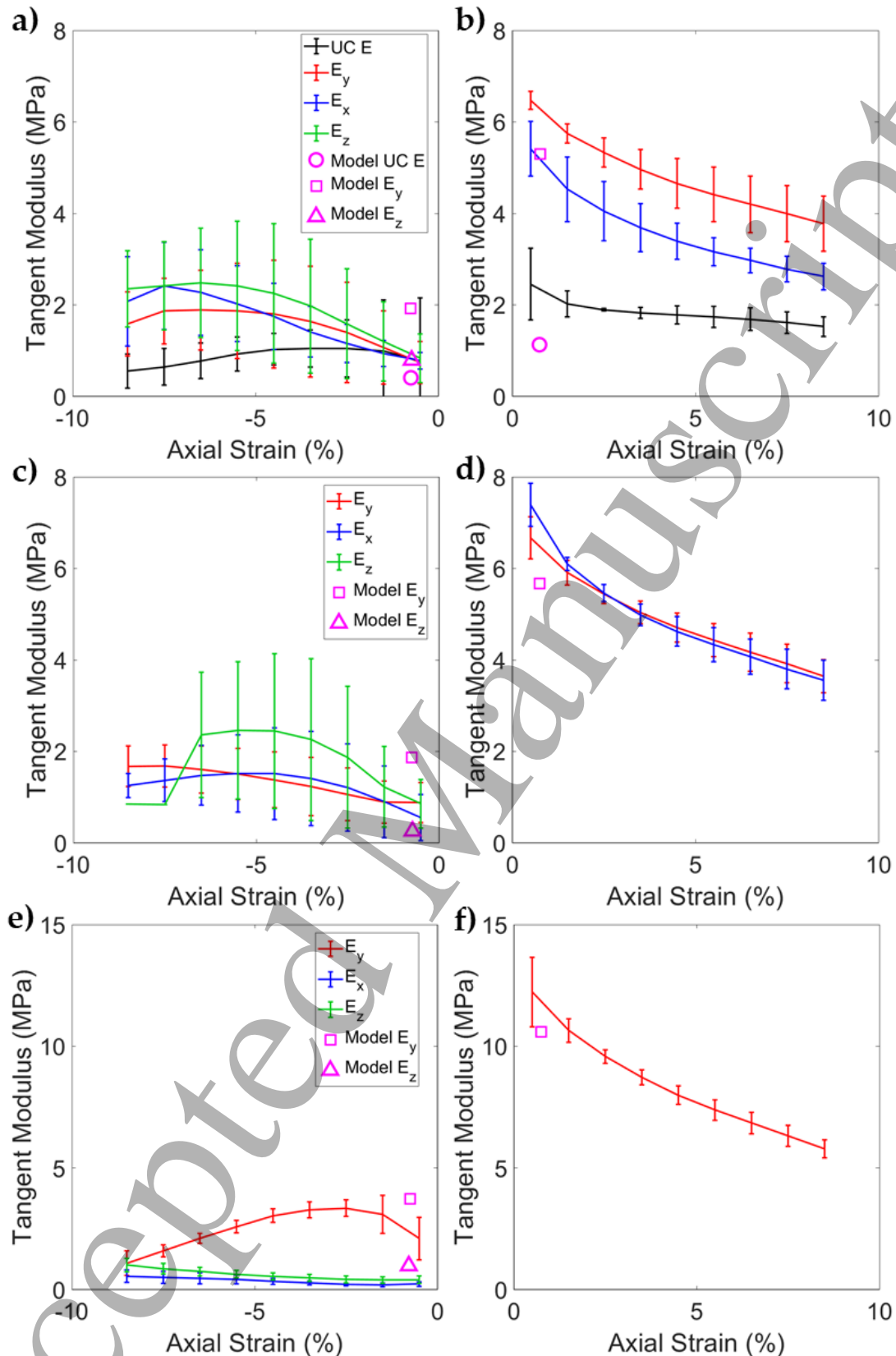


329
 330 **Figure 7.** Measured and calculated (Equation 4) Poisson's ratio vs. axial strain for; a) & b) unconverted and
 331 unconstrained foam (samples from the gradient sheet, a) in compression, b) in tension), c) & d) constrained foam
 332 from the gradient sheet (c) in compression, d) in tension), e) & f) the stretched section of the gradient cuboid
 333 sample (e) in compression, f) in tension). Data for axial and transverse strain parallel to the x and y-axis or at 45°
 334 were combined. Mean values and error bars showing 1 S.D. are plotted, except for in (e) where median values
 335 were plotted in compression. Legends in a), c) & e) apply to b), d) & f), respectively. All samples and orientations
 336 are included in Supplementary material S1 and data is also included in Table S1.

3.6 Tangent moduli

Unconverted foam exhibited tangent moduli of ~1 MPa up to ~5% compression (Figure 8a), with a reduction to ~0.5 MPa when it entered the plateau region (Figure 6c), and of ~2.5 MPa up to 10% tension (Figure 8b). In compression, both regions of the gradient sheet (Figures 8a & c) were stiffer through thickness ($E_y \approx 2.5$ MPa at 5% compression) than in plane (E_x & $E_y \approx 1$ to 1.5 MPa). Planar tensile Young's moduli were lower in the unconstrained region (E_x & $E_y \approx 7$ MPa, Figure 8b) than the constrained region (E_x & $E_y \approx 8$ MPa, Figure 8d). Compressive tangent moduli parallel to the x and y-axis tended to be higher in the constrained region (~1 to 2 MPa, Figure 8c) than the unconstrained region (~0.5 to 1.5 MPa, Figure 8a), but lower (both ~1 to 2 MPa) when loaded parallel to the z-axis. When loaded along the stretched (y) axis, the stretched region of the gradient cuboid was stiffer (Figure 8e & f) than other orientations and samples; both in compression (tangent modulus up to 4 MPa, Figure 8e) and tension ($E_y \approx 12$ MPa, Figure 8f), agreeing with trends in previous work stretching open cell foam during fabrication [40,56]. Young's moduli are also in Supplementary Table S1.

Differences in both tensile and compressive tangent moduli between regions agree with increased anisotropy in Poisson's ratio measurements (Figure 7), micro-ct images of cell structures (Figure 4), LCRs (Figure 3) and the analytical model (Figure 8). Equation 3 also predicts Young's moduli to within ~1 S.D. of the mean measured value (Figure 8). As with Poisson's ratio measurement and calculations, the lower stiffness in tension supports increased cell wall flexure and bending in compression.



357
 358 **Figure 8.** Mean and calculated (Equation 3) tangent moduli of a) & b) unconstrained and unconverted foam
 359 (samples from the gradient sheet) in a) compression and b) tension; c) & d) the constrained section of the gradient
 360 sheet in c) compression and d) tension; e) & f) the stretched section of the gradient cuboid in e) compression and
 361 f) tension. Error bars show 1 S.D. All samples and fabrication shown in Supplementary material S1, and data is
 362 replicated in Table S1.

363 4. Discussion

364 Constraining, stretching or preventing steam from reaching regions of closed cell foam
365 allowed control over cell structure during steam conversions (Figure 3). Constraining and
366 stretching foam regions during fabrication increased anisotropy in gradient foam regions.
367 Comparison with an analytical model, adapted from previous works [40,51], showed
368 agreement (within ~ 1 S.D.) between imparted LCRs (Figure 3) and cell structures (Figure 4),
369 with measured Poisson's ratios (Figure 7) and Young's moduli (Figure 8). The imparted cell
370 structures of regions of auxetic foam that were unconstrained during fabrication look similar
371 to those in previous work, and agree with an analytical model [48,49]. Further work could
372 steam larger and thicker samples of constrained foam, to allow for compression tests that
373 comply with ASTM D3574 – 11 [53].

374 Regions of foam unconstrained during fabrication, from different samples, exhibited
375 similar mechanical properties, including Poisson's ratios (lowest $\nu_{yz} \approx -0.7$, Figure 7, Figure
376 S1) and tensile Young's moduli of ~ 7 MPa (Figure 8b, Figure S2). The gradient sheet had a
377 slight gradient along its y-axis (e.g. $\nu_{yz} \approx -0.7$ to -0.8 , tensile $E_y \approx 7$ to 8 MPa), as expected and
378 predicted by the analytical model (Figures 7c, 7d, 8c, 8d). The two cuboids had clear gradients
379 between regions: i) Unconstrained regions were similar (e.g. $\nu_{yz} \approx -0.7$, tensile $E_y \approx 7$ MPa); ii)
380 The stretched region had similar tensile ν_{yz} of ~ -0.5 (Figures 7c) but higher tensile E_y of ≈ 12
381 MPa (Figure 8f); iii) The dry-heated region was similar to the unconverted foam (Figures 7a,
382 7b, 8a, 8b), with $\nu \approx 0.4$ and $E \approx 2.5$ MPa (Figures S1f and S2f).

383 The effects of modifying cell structure agreed with our understanding of open and
384 closed cell foam, including; i) analytical models of auxetic and conventional open cell foam
385 [40,41,50]; ii) analytical models of conventional closed cell foam [41,51,52], and; iii) previous
386 tests of auxetic closed cell foam [47–49]. Cell structure (Figure 4h) and Poisson's ratio (Figure
387 7a & b) in directions constrained (LCRs = 1), but not stretched, by pins during steaming were
388 similar to that of the unconverted foam. Young's moduli of the converted foam did, however,

1
2
3 389 tend to increase with foam density from shrinkage in the unconstrained through thickness
4
5 390 direction (Figures 3a, 8a & 8b). Kinked cell walls and smaller cells imparted by the steam
6
7 391 process (Figure 4e & f) gave NPR (Figure 7a & b) and increased Young's modulus (Figure 8a
8
9 392 & b), as in previous work with open cell foam [19,23,38,40].

10
11
12 393 Considering the gradient sheet, constraining the foam (and cells) during fabrication, and
13
14 394 volumetric shrinking during cooling - when the polyethylene was softened by the remaining
15
16 395 heat - is likely to have increased the diagonal rib length (i.e. l in Figure S3). Increasing the
17
18 396 relative diagonal cell wall length in the analytical model increased transverse strain ($\epsilon_{\text{transverse}} \propto$
19
20 397 l/h , whereby h is vertical rib length, Supplementary Figure S3) and the magnitude of cellular
21
22 398 NPR (ν_{yz} , Figure S7a), agreeing with mechanical test data and clearest in tension (e.g. Figure
23
24 399 7a to d). The increased magnitude of NPR would, then, be expected to increase volumetric
25
26 400 deformation, and therefore changes in internal air pressure, increasing stiffness ($E_{\text{combined}} \propto E_{\text{air}}$
27
28 401 $\propto \epsilon_v$, Equation 2), as in Figure 8a to d [51].

29
30
31 402 Compressive and tensile characteristics of the steamed foams differed, depending on
32
33 403 the specifics of fabrication. NPR was maintained to higher tension (10%) than compression
34
35 404 (~2%, Figure 7), suggesting more implications for fit of personal protective equipment, and
36
37 405 prosthetics, than indentation or impact performance, although this was not tested specifically.
38
39 406 Previous work suggested that cell wall buckling began at low (0 to 3%) compression of closed
40
41 407 cell foams [51]. The analytical model (Equations 3 & 4) predicts negative tensile Poisson's
42
43 408 ratio (ν_{yz}), but near zero or positive compressive Poisson's ratio (ν_{yz} , Figure 7), and reduced
44
45 409 compressive stiffness (E_y , Figure 8), as cell walls buckle. Lengthening cells, by stretching foam
46
47 410 in the y-axis during fabrication (Figure 4j), increased stiffness in the y-axis (E_y , Figure 8e & f)
48
49 411 [23,57], and gave positive compressive Poisson's ratio (Figure 7e).

50
51
52 412 Before considering internal air pressure, the analytical model and previous work in open
53
54 413 cell foam [40], suggest compressive NPR, and low compressive transverse stiffness, as cell

1
2
3 414 wall flexure and bending increase (Figure S5, [40]). With their low transverse stiffness, air
4
5 415 trapped in the cells caused transverse expansion and positive compressive Poisson's ratio
6
7 416 (Figure 7 and Equation 4). The effect of air pressure in the closed cells, and the compression
8
9 417 level at which positive Poisson's ratio occurred (Figure 7a, c & e), increased with the diagonal
10
11 418 cell wall length (Supplementary Figure S3 b to d), as relative transverse stiffness decreased
12
13 419 (Figure 8) [40]. Further work could develop this auxetic closed cell foam analytical model for
14
15 420 larger strains.

16
17
18
19 421 Unlike most auxetic open cell foams, the closed cell auxetic foams reported here had
20
21 422 similar compressive stiffness (~1 to 4 MPa, Figure 8a) to foam in personal protective
22
23 423 equipment (~1 MPa [58–60]), running shoe midsoles (~2 MPa [33,61]) liners for prosthetic
24
25 424 sockets (~1 MPa [62]) and expanded foam in helmets (~5 to 20 MPa [63–65]). Foams
26
27 425 fabricated herein also had a wide range of tensile moduli (5 to 12 MPa, Figure 8), similar to
28
29 426 that of expanded foam used in helmets. These foams were up to twice as stiff as similar foam
30
31 427 fabricated without constraints [49]. While similar stiffness open cell auxetic foams have been
32
33 428 fabricated before [31], these closed cell auxetic foams have higher porosity (FDRs up to 5,
34
35 429 Figure 3, than $FDR \approx 10$ in previous work [31]), and high magnitude NPR during loading in
36
37 430 the same axes as their desirable Young's moduli (~1 to 12 MPa, Figures 7 & 8). Alignment of
38
39 431 desirable characteristics (NPR and Young's modulus), and high porosity, mean these auxetic
40
41 432 closed cell foams could realise the previously demonstrated [4–6,8,28,37,66] and discussed
42
43 433 [30,67–69] benefits of NPR to energy absorption [33,51,58–60,62–65]. The presented methods
44
45 434 facilitate further development and testing, including impact testing at different temperatures
46
47 435 and humidities, of auxetic and gradient foam for often discussed [1,19,30,68], but unrealised,
48
49 436 applications for auxetic foam.

56 437 5. Conclusions

1
2
3 438 We demonstrate control over compression and cell structure during auxetic closed cell
4
5 439 foam fabrications. Poisson's ratios between -1 and 1, compressive tangent moduli from 1 to 4
6
7 440 MPa and tensile Young's moduli between 5 and 12 MPa were shown within a gradient sample.
8
9 441 Obtained mechanical properties agree (within ~1 S.D.) with analytical models adapted from
10
11 442 previous models for auxetic open cell and conventional closed cell foam. Open cell gradient
12
13 443 auxetic foam is available, but typically with Young's moduli at least ten times lower than that
14
15 444 of the closed cell foams presented here. Now that such control is possible during closed cell
16
17 445 auxetic and gradient foam fabrications, prototype devices featuring auxetic and gradient foam,
18
19 446 such as sporting personal protective equipment, helmets, prosthetics and footwear, can be
20
21 447 developed and tested. Future work could impact test the foams developed here for such
22
23 448 applications. The development of an analytical model for auxetic closed cell foam provides a
24
25 449 better understanding of such foams, which could help in their application to sports equipment
26
27 450 and other devices.
28
29
30
31
32

33 451 **6. Acknowledgements**

34 452 The work was funded by Manchester Metropolitan University's Strategic Opportunities
35
36 453 Fund, and Sheffield Hallam University's Creating Knowledge Investment Platform.
37
38 454 Characterisation, testing, writing and analysis was under taken by Dr. Duncan, with equal
39
40 455 guidance given by both co-authors.
41
42
43
44

45 456 **7. References**

- 46 457 1. Lakes RS. Foam Structures with a Negative Poisson's Ratio. *Science* (80-). 1987.235(4792).
47 458 1038–40.
48 459 2. Cross TM, Hoffer KW, Jones DP, Kirschner PB, Meschter JC. Auxetic Structures And
49 460 Footwear With Soles Having Auxetic Structures (US 2015/0075034 A1). Vol. 1. 2015.
50 461 3. Moroney C, Alderson A, Allen T, Sanami M, Venkatraman P. The Application of Auxetic
51 462 Material for Protective Sports Apparel. *Proceedings*. 2018.2(6). 251.
52 463 4. Chan N, Evans KE. Indentation resilience of conventional and auxetic foams. *J Cell Plast*.
53 464 1998.34. 231–60.
54 465 5. Lakes RS, Elms K. Indentability of conventional and negative Poisson's ratio foams. *J*
55 466 *Compos Mater*. 1993.27(12). 1193–202.
56 467 6. Ge C. A comparative study between felted and triaxial compressed polymer foams on cushion
57 468 performance. *J Cell Plast*. 2013.49(6). 521–33.
58 469 7. Lisiecki J, Błazejewicz T, Kłysz S, Gmurczyk G, Reymer P, Mikułowski G. Tests of
59 470 polyurethane foams with negative Poisson's ratio. *Phys Status Solidi Basic Res*. 2013.250(10).

- 1
2
3 471 1988–95.
- 4 472 8. Allen T, Shepherd J, Hewage TAM, Senior T, Foster L, Alderson A. Low-kinetic energy
5 473 impact response of auxetic and conventional open-cell polyurethane foams. *Phys Status Solidi*
6 474 *Basic Res.* 2015.9. 1–9.
- 7 475 9. Scarpa F, Ciffo LG, Yates JR. Dynamic properties of high structural integrity auxetic open cell
8 476 foam. *Smart Mater Struct.* 2003.13(1). 49–56.
- 9 477 10. Scarpa F, Pastorino P, Garelli A, Patsias S, Ruzzene M. Auxetic compliant flexible PU foams:
10 478 Static and dynamic properties. *Phys Status Solidi Basic Res.* 2005.242(3). 681–94.
- 11 479 11. Scarpa F, Giacomini J, Zhang Y, Pastorino P. Mechanical performance of auxetic polyurethane
12 480 foam for antivibration glove applications. *Cell Polym.* 2005.24(5). 253–68.
- 13 481 12. Li Q, Yang D. Vibro-acoustic performance and design of annular cellular structures with
14 482 graded auxetic mechanical metamaterials. *J Sound Vib [Internet].* 2020.466. 115038.
15 483 Available from: <https://doi.org/10.1016/j.jsv.2019.115038>
- 16 484 13. Li Q, Yang D. Vibration and Sound Transmission Performance of Sandwich Panels with
17 485 Uniform and Gradient Auxetic Double Arrowhead Honeycomb Cores. *Shock Vib.* 2019.2019.
- 18 486 14. Howell B, Prendergast P, Hansen L. Examination of acoustic behavior of negative poisson's
19 487 ratio materials. *Appl Acoust.* 1994.43(2). 141–8.
- 20 488 15. Almutairi MM, Osman M, Tlili I. Thermal Behavior of Auxetic Honeycomb Structure: An
21 489 Experimental and Modeling Investigation. *J Energy Resour Technol Trans ASME.*
22 490 2018.140(12).
- 23 491 16. Innocenti P, Scarpa F. Thermal conductivity properties and heat transfer analysis of Multi-re-
24 492 entrant auxetic honeycomb structures. *J Compos Mater.* 2009.43(21). 2419–39.
- 25 493 17. Chun Checn H, Scarpa F, Hallak Panzera T, Farrow I, Peng H-X. Shear stiffness and energy
26 494 absorption of auxetic open cell foams as sandwich cores. *Phys Status Solidi.* 2018.256(1). 1–9.
- 27 495 18. Timoshenko SP, Goodier JN. *Theory of Elasticity.* 3rd ed. New York: McGraw-Hill, USA;
28 496 1970.
- 29 497 19. Alderson A, Alderson KL, McDonald SA, Mottershead B, Nazare S, Withers PJ, et al.
30 498 Piezomorphic materials. *Macromol Mater Eng.* 2013.298(3). 318–27.
- 31 499 20. Evans KE. The design of doubly curved sandwich panels with honeycomb cores. *Compos*
32 500 *Struct.* 1991.17(2). 95–111.
- 33 501 21. Chan N, Evans KE. Fabrication methods for auxetic foams. *J Mater Sci.* 1997.32. 5945–53.
- 34 502 22. Li Y, Zeng C. Room-Temperature, Near-Instantaneous Fabrication of Auxetic Materials with
35 503 Constant Poisson's Ratio over Large Deformation. *Adv Mater.* 2016.28(14). 2822–6.
- 36 504 23. Sanami M, Alderson A, Alderson KL, McDonald S a., Mottershead B, Withers PJ. The
37 505 production and characterization of topologically and mechanically gradient open-cell
38 506 thermoplastic foams. *Smart Mater Struct.* 2014.23(5). 055016.
- 39 507 24. Lowe A, Lakes RS. Negative Poisson's ratio foam as seat cushion material. *Cell Polym.*
40 508 2000.19(3). 157–67.
- 41 509 25. Stojmanovski Mercieca LA, Formosa C, Grima JN, Chockalingam N, Gatt R, Gatt A. On the
42 510 Use of Auxetics in Footwear: Investigating the Effect of Padding and Padding Material on
43 511 Forefoot Pressure in High Heels. *Phys Status Solidi Basic Res.* 2017.254(12). 1–5.
- 44 512 26. Allen T, Duncan O, Foster L, Senior T, Zampieri D, Edeh V, et al. Auxetic foam for snow-
45 513 sport safety devices. *Snow Sport Trauma Saf Proc Int Soc Ski Saf.* 2016.21.
- 46 514 27. Foster L, Peketi P, Allen T, Senior T, Duncan O, Alderson A. Application of Auxetic Foam in
47 515 Sports Helmets. *Appl Sci.* 2018.8(3). 354.
- 48 516 28. Duncan O, Foster L, Senior T, Alderson A, Allen T. Quasi-static characterisation and impact
49 517 testing of auxetic foam for sports safety applications. *Smart Mater Struct.* 2016.25(5). 054014.
- 50 518 29. Critchley R, Corni I, Wharton JA, Walsh FC, Wood RJK, Stokes KR. A review of the
51 519 manufacture, mechanical properties and potential applications of auxetic foams. *Phys Status*
52 520 *Solidi Basic Res.* 2013.250(10). 1963–82.
- 53 521 30. Duncan O, Shepherd T, Moroney C, Foster L, Venkatraman PD, Winwood K, et al. Review of
54 522 auxetic materials for sports applications: Expanding options in comfort and protection. *Appl*
55 523 *Sci.* 2018.8(6). 941.
- 56 524 31. Zhang Q, Lu W, Scarpa F, Barton D, Lakes RS, Zhu Y, et al. Large stiffness thermoformed
57 525 open cell foams with auxeticity. *Appl Mater Today.* 2020.20. 100775.

- 1
2
3 526 32. Ankrah S, Mills NJ. Analysis of ankle protection in Association football. *Sport Eng.*
4 527 2004.7(1). 41–52.
- 5 528 33. Mills NJ, Fitzgerald C, Gilchrist A, Verdejo R. Polymer foams for personal protection:
6 529 Cushions, shoes and helmets. *Compos Sci Technol.* 2003.63(16). 2389–400.
- 7 530 34. Mills NJ. The biomechanics of hip protectors. *Proc Inst Mech Eng H.* 1996.210(4). 259–66.
- 8 531 35. Duncan O, Clegg F, Essa A, Bell AMT, Foster L, Allen T, et al. Effects of Heat Exposure and
9 532 Volumetric Compression on Poisson's Ratios, Young's Moduli, and Polymeric Composition
10 533 During Thermo-Mechanical Conversion of Auxetic Open Cell Polyurethane Foam. *Phys*
11 534 *Status Solidi.* 2019.
- 12 535 36. Grima JN, Attard D, Gatt R. A novel process for the manufacture of auxetic foams and for the
13 536 conversion of auxetic foam to conventional form (WO 2010049511 A2). 2010. 1–5.
- 14 537 37. Lisiecki J, Klysz S, Blazejowicz T, Gmurczyk G, Reymer P. Tomographic examination of
15 538 auxetic polyurethane foam structures. *Phys Status Solidi Basic Res.* 2013.251(2). 314–20.
- 16 539 38. Alderson A, Davies PJ, Alderson KIML, Smart GM. The Effects of Processing on the
17 540 Topology and Mechanical Properties of Negative Poisson's Ratio Foams. *Proc IMECE2005*
18 541 *2005 ASME Int Mech Eng Congr Expo Proc IMECE200.* 2005. 1–8.
- 19 542 39. Bianchi M, Scarpa F, Banse M, Smith CW. Novel generation of auxetic open cell foams for
20 543 curved and arbitrary shapes. *Acta Mater.* 2011.59(2). 686–91.
- 21 544 40. Duncan O, Allen T, Foster L, Senior T, Alderson A. Fabrication, characterisation and
22 545 modelling of uniform and gradient auxetic foam sheets. *Acta Mater.* 2017.126. 426–37.
- 23 546 41. Gibson LJ, Ashby MF. Cellular solids. Structure and properties. **1997.** 67, 176–183, 259–264,
24 547 286, 301, 498 p.
- 25 548 42. Imam S, Driscoll H, Winwood K, Venkatraman P, Allen T. Efficacy of Density in Predicting
26 549 the Protective Properties of Padded Clothing in Rugby †. *Proc 13th Conf Int Sport Eng Assoc.*
27 550 *2020.49(38).* 1–7.
- 28 551 43. Mills NJ. Foam protection in sport. In: Jenkins M, editor. *Materials in sports equipment.*
29 552 *Volume 1.* Cambridge, UK: Woodhead Publishing Limited; **2003.** p. 20–9.
- 30 553 44. Mawkhlieng U, Majumdar A. Soft body armour. *Text Prog.* 2019.51(2). 139–224.
- 31 554 45. Sterzing T, Custozza G, Ding R, Cheung JTM. Segmented midsole hardness in the midfoot to
32 555 forefoot region of running shoes alters subjective perception and biomechanics during heel-toe
33 556 running revealing potential to enhance footwear. *Footwear Sci.* 2015.7(2). 63–79.
- 34 557 46. Mohsenizadeh S, Ahmad Z, Alipour R, Majid RA, Prawoto Y. Quasi Tri-Axial Method for the
35 558 Fabrication of Optimized Polyurethane Auxetic Foams. *Phys Status Solidi.* 2019.1800587.
36 559 1800587.
- 37 560 47. Martz EO, Lee T, Lakes RS, Goel VK, Park JB. Re-entrant transformation methods in closed
38 561 cell foams. *Cell Polym.* 1996.15(4). 229–49.
- 39 562 48. Fan D, Li M, Qiu J, Xing H, Jiang Z, Tang T. Novel Method for Preparing Auxetic Foam from
40 563 Closed-Cell Polymer Foam Based on the Steam Penetration and Condensation Process. *ACS*
41 564 *Appl Mater Interfaces.* 2018.
- 42 565 49. Duncan O, Birch A, Allen T, Foster L, Hart J, Alderson A. Effect of steam conversion on the
43 566 cellular structure, Young's modulus and negative Poisson's ratio of closed cell foam. *Smart*
44 567 *Mater Struct.* 2020.((Accepted)).
- 45 568 50. Masters IG, Evans KE. Models for the elastic deformation of honeycombs. *Compos Struct.*
46 569 *1996.35(4).* 403–22.
- 47 570 51. Mills NJ, Zhu HX. The high strain compression of closed-cell polymer foams. *J Mech Phys*
48 571 *Solids.* 1999.47(3). 669–95.
- 49 572 52. Rusch KC. Load-compression behavior of brittle foams. *J Appl Polym Sci.* 1970.14(5). 1263–
50 573 76.
- 51 574 53. Annual Book of ASTM Standards. Standard Test Methods for Flexible Cellular Materials —
52 575 Slab, Bonded, and Molded Urethane Foams. Annual Book of ASTM Standards 2008.
- 53 576 54. Wang D, Diazdelao FA, Wang W, Lin X, Patterson EA, Mottershead JE. Uncertainty
54 577 quantification in DIC with Kriging regression. *Opt Lasers Eng.* 2016.78. 182–95.
- 55 578 55. Mills NJ, Gilchrist A. Modelling the indentation of low density polymer foams. *Cell Polym.*
56 579 *2000.19(6).* 389–412.
- 57 580 56. Ramaswamy H. Fabrication and testing of 2-dimensional Z-expandable auxetic textile

- 1
2
3 581 structures for impact protective clothing applications. 2014. 1–15.
4 582 57. Allen T, Hewage T, Newton-Mann C, Wang W, Duncan O, Alderson A. Fabrication of
5 583 Auxetic Foam Sheets for Sports Applications. *Phys Status Solidi Basic Res.* 2017.1700596. 1–
6 584 6.
7 585 58. Signetti S, Nicotra M, Colonna M, Pugno NM. Modeling and simulation of the impact
8 586 behavior of soft polymeric-foam-based back protectors for winter sports. *J Sci Med Sport.*
9 587 2018.
10 588 59. Nicotra M, Moncalero M, Messori M, Fabbri E, Fiorini M, Colonna M. Thermo-mechanical
11 589 and impact properties of polymeric foams used for snow sports protective equipment. *Procedia*
12 590 *Eng.* 2014.72. 678–83.
13 591 60. Ankrah S, Mills NJ. Performance of football shin guards for direct stud impacts. *Sport Eng.*
14 592 2003.6(4). 207–19.
15 593 61. Verdejo R, Mills NJ. Heel-shoe interactions and the durability of EVA foam running-shoe
16 594 midsoles. *J Biomech.* 2004.37(9). 1379–86.
17 595 62. Sanders JE, Greve JM, Mitchell SB, Zachariah SG. Material properties of commonly-used
18 596 interface materials and their static coefficients of friction with skin and socks. *J Rehabil Res*
19 597 *Dev.* 1998.35(2). 161–76.
20 598 63. Krundaeva A, De Bruyne G, Gagliardi F, Van Paepegem W. Dynamic compressive strength
21 599 and crushing properties of expanded polystyrene foam for different strain rates and different
22 600 temperatures. *Polym Test.* 2016.55(2016). 61–8.
23 601 64. Mosleh Y, Bosche K Vanden, Sloten J Vander, Verpoest I, Ivens J. Combined shear-
24 602 compression test to characterize foams under oblique loading for bicycle helmets. In: In
25 603 Proceedings of the 16rd European Conference on Composites Materials ECCM16, Seville,
26 604 Spain. 2014. p. 22–6.
27 605 65. Andena L, Caimmi F, Leonardi L, Ghisi A, Mariani S, Braghin F. Towards Safer Helmets:
28 606 Characterisation, Modelling and Monitoring. *Procedia Eng.* 2016.147. 478–83.
29 607 66. Pastorino P, Scarpa F, Patsias S, Yates JR, Haake SJ, Ruzzene M. Strain rate dependence of
30 608 stiffness and Poisson's ratio of auxetic open cell PU foams. *Phys Status Solidi Basic Res.*
31 609 2007.244(3). 955–65.
32 610 67. Novak N, Vesenjask M, Ren Z. Auxetic cellular materials - A review. *Stroj Vestnik/Journal*
33 611 *Mech Eng.* 2016.62(9). 485–93.
34 612 68. Evans KE, Alderson A. Auxetic materials: Functional materials and structures from lateral
35 613 thinking! *Adv Mater.* 2000.12(9). 617–28.
36 614 69. Yang W, Li ZM, Shi W, Xie BH, Yang MB. On auxetic materials. *J Mater Sci.* 2004.39(10).
37 615 3269–79.
38 616
39 617
40
41
42
43
44
45
46
47
48
49
50
51
52
53
54
55
56
57
58
59
60